

Numerical simulation of free-surface waves past two semi-submerged horizontal circular cylinders in tandem

Muk Chen Ong^{a*}, Arun Kamath^b, Hans Bihs^b, Mohammad Saud Afzal^c

^aDepartment of Mechanical and Structural Engineering and Materials Science, University of Stavanger, 4036 Stavanger, Norway

^bDepartment of Civil and Transport Engineering, Norwegian University of Science and Technology (NTNU), 7491 Trondheim, Norway

^cDepartment of Marine Technology, Norwegian University of Science and Technology (NTNU), 7491 Trondheim, Norway

Marine Structures, 2017, **52**, pp. 1-14.

DOI: <http://dx.doi.org/10.1016/j.marstruc.2016.11.002>

Abstract

Two-dimensional (2D) numerical simulations are performed to investigate free surface waves past two semi-submerged horizontal circular cylinders in tandem. The 2D simulations are carried out by solving the Unsteady Reynolds-Averaged Navier-Stokes (URANS) equations with the k - ω turbulence model. The level set method is employed to model the free-surface waves. Validation studies of a numerical wave tank have been performed by comparing the numerical simulations with free-surface waves past a partially-submerged horizontal cylinder with the published experimental data under regular-wave and deep water conditions. Cases with different submerged depths of the cylinder and incident wave properties have been studied. The numerical results are in good agreement with the experimental measurement in terms of hydrodynamic forces. Subsequently, free surface waves past two semi-submerged horizontal cylinders in tandem are computed numerically. The effect of spacing between the two cylinders is investigated by examining the changes in the vertical hydrodynamic forces on and the free surface elevations around the cylinders.

Keywords: free surface waves; partially submerged horizontal cylinders; hydrodynamic forces; REEF3D; Computational Fluid Dynamics

*Corresponding author, muk.c.ong@uis.no

Postprint, published in *Marine Structures*, doi:<http://dx.doi.org/10.1016/j.marstruc.2016.11.002>

1 Introduction

Partially-submerged bluff bodies are often found in offshore and marine structures, e.g., wave energy converters, semisubmersible platforms and fish cages. Circular cylinders are usually one of the important components in these structures. Free surface flow around partially-submerged fixed circular cylinders is hard and expensive to achieve in an experimental setup, which requires appropriate experimental facilities (e.g. a well-designed wave tank), minimizing human and instrument errors during measuring hydrodynamic quantities etc. Therefore an attractive alternative is to use Computational Fluid Dynamics (CFD) to obtain the essential hydrodynamic quantities needed for engineering design. The wave condition and the submerged depth of the cylinder play important roles in determining the hydrodynamic forces and the flow structures.

Several sets of experimental data for free surface past a partially-submerged fixed circular cylinder have been published in the open literature. Dixon et al. (1979) carried out experiments to measure regular wave forces on a partially-submerged fixed cylinder at low Keulegan-Carpenter (KC) numbers ranging from 0.6 to 3.1. They measured the vertical forces acting on the cylinder for different levels of submergence and wave amplitude. They found that the interplay between inertia and buoyancy leads to entirely negative heave forces which act at twice the wave frequency, under certain situations. Prasad (2011) investigated the slamming force due to non-breaking and breaking wave impact on a fixed horizontal cylinder near the still water level. The vertical force data were analyzed to obtain the corresponding slamming and impulse coefficients. Eason et al. (1985) measured the force spectra from partially submerged circular cylinders in random seas.

Not many Computational Fluid Dynamic (CFD) simulations have been performed to predict wave loads on a partially submerged fixed circular cylinder. Westphalen et al. (2009) and Hu et al. (1985) validated their CFD solvers for wave energy converters by studying wave loads on the partially submerged cylinders. They compared their numerical results with some selected experimental data from Dixon et al. (1979). Turbulence contribution was not included in their numerical studies. Westphalen et al. (2009) reported that the CFD results give good comparison with the experimental data when the cylinder is partially submerged. However, the relative forces calculated by CFD are not in good agreement with the experimental data for the fully submerged case.

To the authors' knowledge, there are no published experimental or numerical studies on the free surface waves past two semi-submerged horizontal circular cylinders in tandem. The main objectives of the present study are to evaluate whether a level set method based numerical wave tank is applicable for this type of engineering application and study the hydrodynamic quantities on both a single partially submerged cylinder and two semi-submerged cylinders in tandem. The open-source CFD model REEF3D applied to various marine engineering problems such as the study of breaking waves (Alagan Chella et al., 2015*a,b*), wave forces on cylinders (Kamath et al., 2015*a*) and renewable energy devices (Kamath et al., 2015*b*) is used in the present study. First, the free surface flows around a partially-submerged circular cylinder in linear free surface waves with different submerged depth are investigated numerically. The numerical results will be compared with the published experimental results; and it will then be considered as a validation study for cases with free surface waves past two semi-submerged cylinders in tandem. The effect of spacing between the two cylinders will be investigated. The hydrodynamic forces on both the upstream and the downstream cylinders

will be computed; and the vertical force on the upstream cylinder will be compared with the numerical results obtained for the corresponding single cylinder case. Changes of the free surface elevation due to the effect of the spacing will also be investigated.

2 Numerical Model and Setup

2.1 Governing Equations

In the present study, a 2D numerical wave tank is employed using REEF3D and the Unsteady Reynolds-averaged Navier Stokes (URANS) equations are solved together with the continuity equation for incompressible flow, prescribing mass and momentum conservation:

$$\frac{\partial u_i}{\partial x_i} = 0 \quad (1)$$

$$\frac{\partial u_i}{\partial t} + u_j \frac{\partial u_i}{\partial x_j} = -\frac{1}{\rho} \frac{\partial p}{\partial x_i} + \frac{\partial}{\partial x_j} \left[(\nu + \nu_t) \left(\frac{\partial u_i}{\partial x_j} + \frac{\partial u_j}{\partial x_i} \right) \right] + g_i \quad (2)$$

where $i, j = 1, 2$. Here x_1 and x_2 denote the horizontal and vertical directions; u_1 and u_2 are the corresponding mean velocity components; ρ is the fluid density ($\rho_{air} = 1.205 \text{ kg/m}^3$, $\rho_{water} = 998.2 \text{ kg/m}^3$); p is the pressure; ν is the kinematic viscosity ($\nu_{air} = 1.41 \times 10^{-5} \text{ m}^2/\text{s}$, $\nu_{water} = 1.004 \times 10^{-6} \text{ m}^2/\text{s}$); ν_t is the eddy viscosity; and g the acceleration of gravity. The numerical model is used as a numerical wave tank. High-order schemes are selected for the current study to avoid unphysical damping of propagating waves. The convection term of the URANS equations is discretized with the Weighted Essentially Non-Oscillatory (WENO) scheme in the conservative finite difference version (Jiang and Shu, 1996). Here, a discretization stencil consists of three sub-stencils, which are weighted according to the local smoothness of the discretised function. The scheme achieves a minimum of 3rd-order accuracy for discontinuous solutions, and up to 5th-order accuracy for a smooth solution. At the same time, a robust numerical stability is achieved, without the negative side effects of numerical limiters. For the time treatment, a third-order accurate total variation diminishing (TVD) Runge-Kutta scheme is employed, consisting of three Euler substeps (Shu and Osher, 1988). The pressure term is solved with the projection method (Chorin, 1968) after each of the Euler substeps for the velocities. The BiCGStab algorithm (van der Vorst H., 1992) with Jacobi scaling preconditioning solves the Poisson equation for the pressure. The URANS equations are closed with the two-equation $k-\omega$ turbulence model (Wilcox, 1994), with transport equations for the turbulent kinetic energy k and the specific dissipation ω . Although the KC numbers are small in the present study, the boundary layer around the cylinders, the flow separation and the vortices formed after the separation could be turbulent when the Reynolds numbers are larger than 10^6 . Moreover, there is overtopping action in the present study; non-linear effect on the free surface is significant.

2.2 Numerical Grid and Parallelisation

At the solid boundaries of the fluid domain a ghost cell immersed boundary method is employed. In this method, the solution is analytically continued through the solid boundary by updating fictitious ghost cells in the solid region through extrapolation. This way, the

numerical discretization does not need to account for the boundary conditions explicitly. The algorithm is based upon the local directional approach by Berthelsen and Faltinsen (2008). With this method, complex geometries and cut cells can be accounted for. The ghost cell approach has several advantages, i.e., : (1) Grid generation becomes trivial; (2) the numerical stability and the order of the overall scheme is not affected; (3) the method integrates well into the domain decomposition strategy for the parallelization of the numerical model. Here ghost cells are used to update the values from the neighbouring processors via MPI (Message Passing Interface).

2.3 Level Set Method

The main feature of wave interaction with partially submerged structures is a complex motion of the free surface. In order to account for this, the interface-capturing level set method is employed, describing the interface between the two phases water and air. With the level set method (Osher and Sethian, 1988), the location of the interface is represented implicitly by the zero level set of the smooth signed distance function $\phi(\vec{x}, t)$. In every point of the computational domain, the level set function gives the closest distance to the interface and the phases are distinguished by the change of the sign. This results in the following properties:

$$\phi(\vec{x}, t) \begin{cases} > 0 \text{ if } \vec{x} \in \text{water} \\ = 0 \text{ if } \vec{x} \in \Gamma \\ < 0 \text{ if } \vec{x} \in \text{air} \end{cases} \quad (3)$$

Also the Eikonal equation $|\nabla\phi| = 1$ is valid. When the interface is moved under an externally generated velocity field \vec{u} , a convection equation for the level set function is obtained:

$$\frac{\partial\phi}{\partial t} + u_j \frac{\partial\phi}{\partial x_j} = 0 \quad (4)$$

With the level set function in place, the material properties of the two phases can be defined for the whole domain. Without special treatment, there is a jump in the density ρ and the viscosity ν across the interface, which can lead to numerical instabilities. This is avoided by smoothing the material properties in the region around the interface with a regularized Heavyside function $H(\phi)$. This region is 2ϵ thick, with ϵ being proportional to the grid spacing Δx . In the present paper it was chosen to be $\epsilon = 2.1\Delta x$. The density and the viscosity can then be written as:

$$\begin{aligned} \rho(\phi) &= \rho_{\text{water}}H(\phi) + \rho_{\text{air}}(1 - H(\phi)), \\ \nu(\phi) &= \nu_{\text{water}}H(\phi) + \nu_{\text{air}}(1 - H(\phi)) \end{aligned} \quad (5)$$

and the regularized Heavyside function:

$$H(\phi) = \begin{cases} 0 & \text{if } \phi < -\epsilon \\ \frac{1}{2} \left(1 + \frac{\phi}{\epsilon} + \frac{1}{\pi} \sin\left(\frac{\pi\phi}{\epsilon}\right) \right) & \text{if } |\phi| < \epsilon \\ 1 & \text{if } \phi > \epsilon \end{cases} \quad (6)$$

2.4 Numerical Wave Tank

A numerical wave tank needs to generate waves at the inlet boundary and absorb waves at the outlet boundary in order to simulate the flow and free surface dynamics of a wave flume. In the present numerical model, the relaxation method is selected for the generation and absorption of waves. The relaxation method concept was first presented by Larsen and Dancy (1983), where the analytical solution is used to moderate the computationally generated waves. This method has been presented by Mayer et al. (1998) and Engsig-Karup (2006). The relaxation function presented by Jacobsen et al. (2012) is used in the present study. In the wave generation relaxation zone, the values for the velocities and the free surface are ramped up from the computational values to the values obtained by wave theory. This generates high quality waves and reflections traveling towards the generation zone are effectively absorbed. In the numerical beach relaxation zone, the computational values for the velocities are smoothly reduced to zero, the free surface modulated to the still water level and the pressure to the according hydrostatic distribution. The wave generation zone is generally kept one wavelength (L) long and the numerical beach is two wavelengths long. The layout of the numerical wave tank with the relaxation zones is presented in Figure 1.

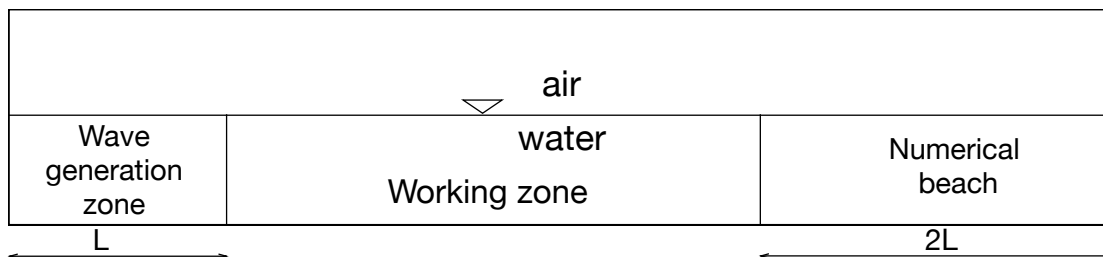


Figure 1: Definition sketch showing the layout of the numerical wave tank with the relaxation zones

2.5 Calculation of Hydrodynamic Force on the Cylinder

The calculation of the wave forces (F) in the numerical model is rather straightforward. The pressure and the wall shear stress are integrated over the surface Ω of the structure of interest. This happens in a discrete fashion, evaluating the pressure p and the wall shear stress tensor τ for each of the structures cell surfaces:

$$F = \int_{\Omega} (-\mathbf{n}p + \mathbf{n} \cdot \boldsymbol{\tau}) d\Omega \quad (7)$$

Because the Navier-Stokes equations in Eqn. (2) are solved including the gravity term, the pressure resulting from the projection method includes the hydrostatic part in addition to the dynamic effects. As a result, it is the total force acting on a structure that is determined by Eqn. (7).

2.6 Simulation Cases

As aforementioned, free surface waves past a partially-submerged circular cylinder and two semi-submerged circular cylinders in tandem will be investigated numerically in the present study. The simulation cases which are performed are shown as follows:

Free Surface Waves past a Partially-Submerged Horizontal Cylinder The definition sketch of free surface waves past a partially-submerged horizontal circular cylinder is shown in Figure 2. Here $a' = a/D$, a = wave amplitude, D = diameter of the cylinder = 1 m, $L' = L/D$, L = wavelength, $d' = d/D$, d = submerged depth of the cylinder and Keulegan Carpenter number $KC = 2\pi a/D$. Deep water linear waves are investigated in the present study. The incident wave properties and the corresponding submerged depth of the cylinder is set up according to the flow conditions reported by Dixon *et al.* (1979). Table 1 shows the incident wave properties and the corresponding submerged depth of the cylinder. The maximum Reynolds number $Re_{max} = u_{max}D/\nu = 10^6$ for $a' = 0.5$ and $L' = 15.62$. Here u_{max} is the undisturbed maximum horizontal water particle velocity at the free surface.

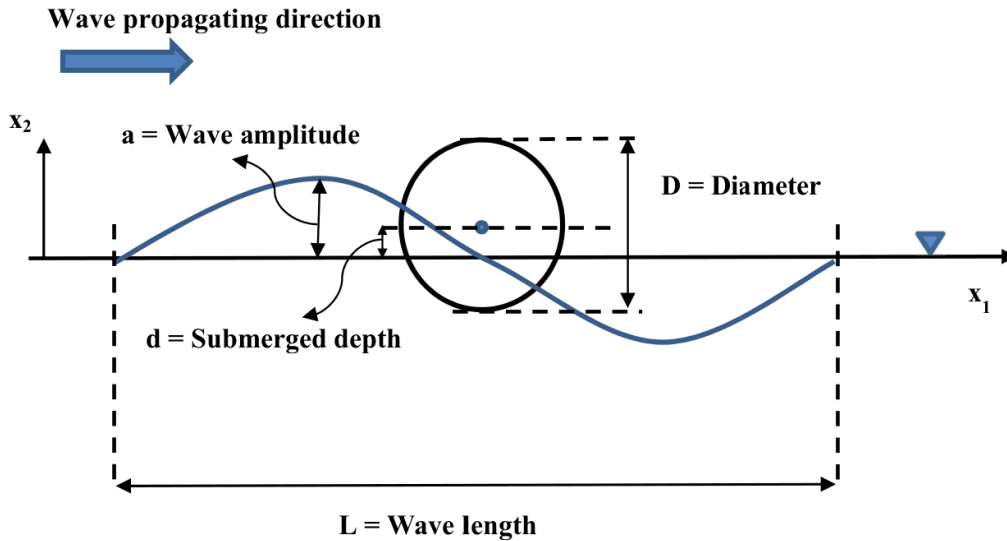


Figure 2: Definition sketch of free surface waves past a partially-submerged horizontal circular cylinder

Free Surface Waves past two Semi-Submerged Horizontal Cylinders in Tandem Free surface waves past two semi-submerged horizontal circular cylinders in tandem are com-

Table 1: Simulation cases for the free surface waves over a partially-submerged cylinder. Here $KC = 2\pi a/D$, $a' = a/D$, $d' = d/D$ and $L' = L/D$.

Index	d'	L'	a'	KC
S1	0.0	15.62	0.5	3.14
S2	0.0	15.62	0.2	1.26
S3	-0.2	15.62	0.2	1.26

puted and discussed in the present study. It should be noted that two cylinders have the same submerged depth. To date, there are no available published experimental or numerical studies on this topic. In order to discuss the simulation results with physical meaning, the incident wave properties and the submerged depth of the cylinders are set up according to Case S1, i.e. $a' = 0.5$, $L' = 15.62$ and $d' = 0.5$; and the spacing between the two cylinders (S) are varied from $1D$ to $15D$, see Figure 3 for the definition sketch. The incident wave condition and the submerged depth ratio for Case S1 ($a' = 0.5$ and $d' = 0$) of the single cylinder study is chosen, because the flow condition is the most complicated among the cases due to the existence of both wave over-topping and wave-run up actions. Table 2 shows the incident wave properties, the submerged depth of the cylinders and different spacing between the two cylinders.

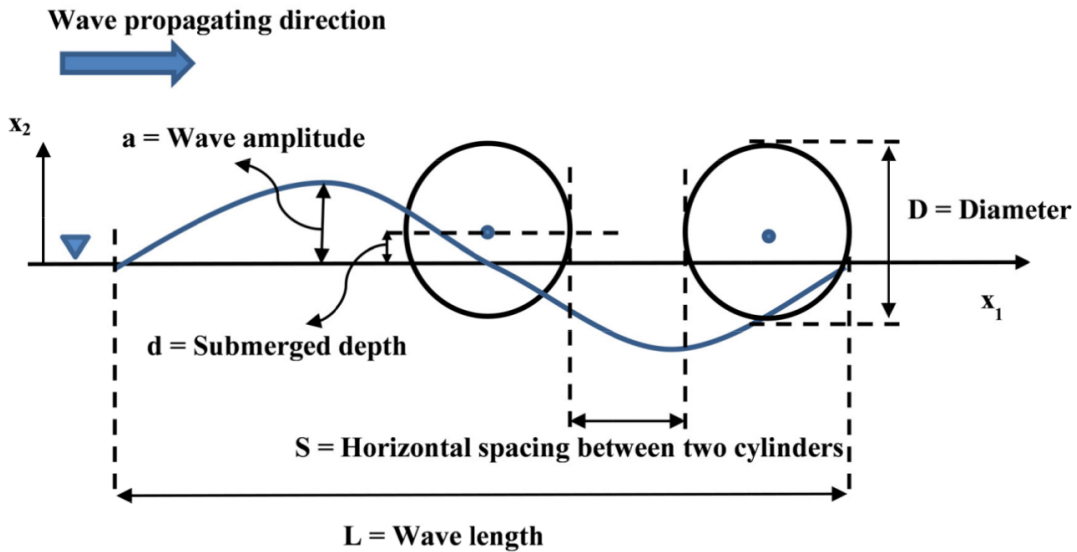


Figure 3: Definition sketch of free surface waves past two Semi-Submerged Horizontal Cylinders in Tandem

Table 2: Simulation cases for the free surface waves over two semi-submerged cylinders.

Index	d'	L'	a'	KC (based on cylinder 1)	S/D
T1	0.0	15.62	0.5	3.14	1
T2	0.0	15.62	0.5	3.14	3
T3	0.0	15.62	0.5	3.14	7
T4	0.0	15.62	0.5	3.14	15

3 Grid Refinement Study

A two-dimensional numerical wave tank is used to perform for a wave force convergence study for free surface waves ($a'=0.5$) past a semi-submerged cylinder ($d'=0.5$), i.e. Case S1. This case is chosen for performing the grid refinement study because the flow condition is the most complicated among the cases (S1-S3) due to effects of both significant wave over-topping and run-up actions. The numerical wave tank is $70D$ long and $12D$ high with a still water level of $8D$. The semi-submerged horizontal cylinder is placed at a horizontal location $30.5D$ away from the inlet.

Figure 4 shows the grid refinement study in term of normalized vertical force F'_v on the cylinder over one wave period. Here dx is the mesh width. The vertical force F_v is defined as follows:

$$F_v = F_{inertial} + F_{buoyancy} \quad (8)$$

$$F'_v = \frac{F_v}{\rho g(\pi D^2/4)} \quad (9)$$

$F_{buoyancy}$ has the initial still water buoyancy removed.

$$F_{buoyancy} = \rho g(V(t) - V_0) \quad (10)$$

$V(t)$ is the instantaneous displaced water volume and V_0 is the initial immersed volume. Three sets of meshes, i.e. Mesh 1 with $dx = 0.1D$ and 84000 elements, Mesh 2 with $dx = 0.05D$ and 336000 elements, Mesh 3 with $dx = 0.025D$ and 1344000 elements, have been tested for the grid refinement study. In the adaptive time stepping scheme, the CFL number is kept constant at 0.1. It appears that Mesh 3 is considered to give sufficient numerical accuracy. This grid resolution (i.e. 625 elements for one wavelength) is used for all the single cylinder simulation cases in the present study.

A similar wave force convergence study has also been performed for free surface waves ($a' = 0.5$) past two semi-submerged cylinders ($d' = 0.5$) i.e. Case T1. Figure 5 shows the grid refinement study in terms of F'_v on each cylinder over one wave period. Three sets of meshes i.e. Mesh 1 with $dx = 0.1D$, Mesh 2 with $dx = 0.05D$ and Mesh 3 with $dx = 0.025D$ have been tested. It appears that Mesh 3 gives sufficient numerical accuracy. This grid resolution (i.e. 625 elements for one wavelength) is used for all the tandem cylinder simulation cases in the present study.

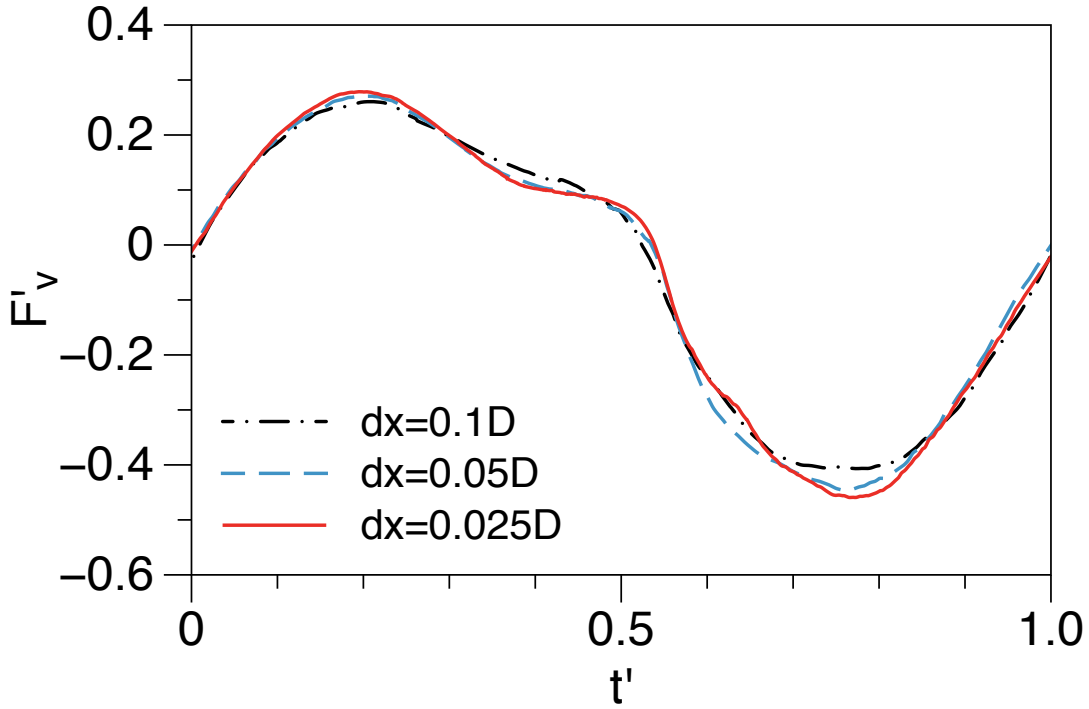


Figure 4: Grid refinement study in term of vertical force F'_v over one wave period for case S1

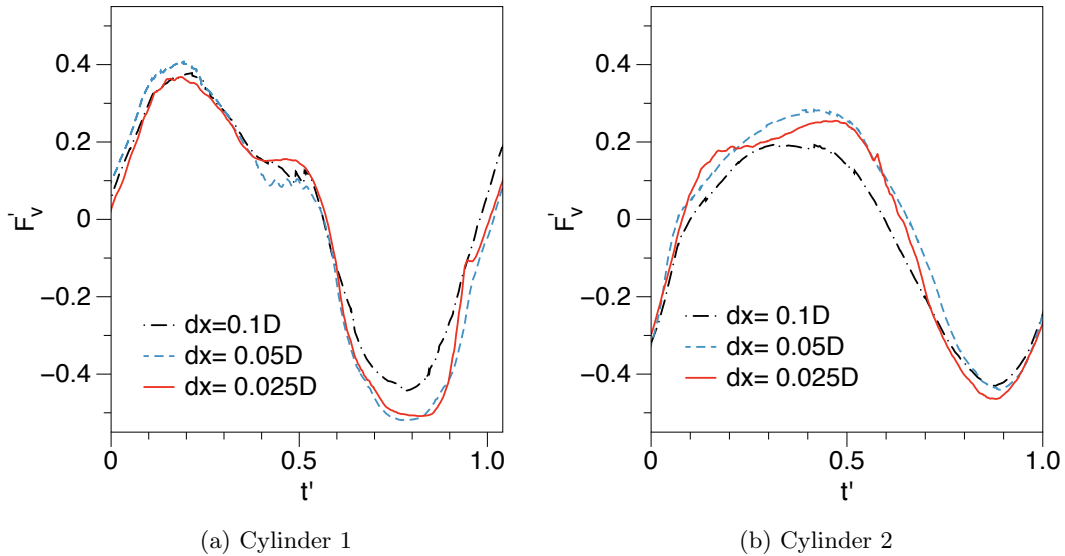


Figure 5: Grid refinement study in term of vertical force F'_v over one wave period for case T1

4 Results and Discussion

4.1 Free Surface Waves past a Partially-Submerged Horizontal Cylinder

As mentioned in Section 2.6.1, three simulations are performed based on the experimental measurement reported by Dixon *et al.* (1979), see Table 1 for the cases and Figure 2 for the

definition sketch.

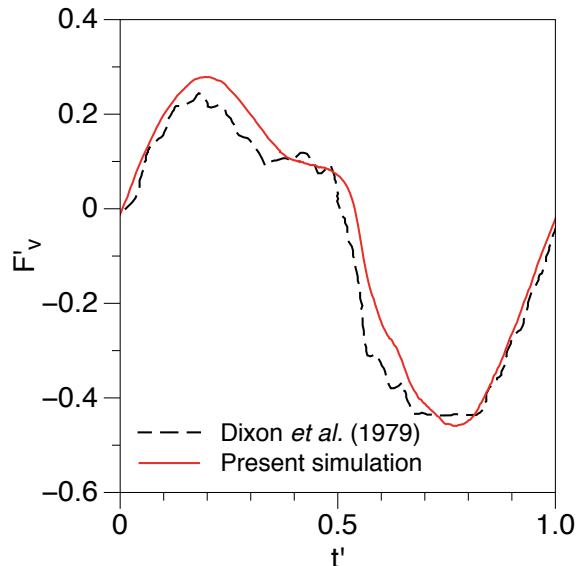


Figure 6: F'_v versus t' over one wave period for Case S1

Figure 6 shows F'_v versus t' over one wave period for Case S1, see Table 1. Here $t' = t/T$, where T is the wave period. Here the wave amplitude is $0.5D$, and it means that the cylinder will have the chance to be fully submerged within every wave period. Both wave over-topping and run-up actions can occur in this case. In Figure 6, the present simulation captures the overall trend of the F'_v distribution over one wave period as compared to the experimental data by Dixon et al. (1979). The feature of asymmetric force distribution over one wave period is well-predicted. There are two peaks in the positive F'_v region for $t' < 0.5$ reported by Dixon et al. (1979), which are mainly due to over-topping wave action on the cylinder. This feature is predicted reasonably well by the present simulation. Figure 7 shows the time history of free surface elevation over a wave period for Case S1 with $t' = (0, 0.12, 0.36, 0.6, 0.73, 1)$. The over-topping and wave run-up actions are clearly shown in the figure. The wave run-up action is clearly observed at $t' = 0.12$ in Figure 7(b); therefore, the largest positive F'_v is observed at the same time in Figure 6. From $t' = 0.3$ to 0.5 , the wave crest is over-topping the cylinder (see Figure 7(c)); the present predicted F'_v agrees well with the experimental results (see Figure 6). At $t' = 0.73$, the wave trough is reaching the bottom of the cylinder. The present model slightly over-predicts the negative F'_v as compared to the experimental data, see Figure 6. Overall, for Case S1, it appears that the present results agrees reasonably well with the experimental data reported by Dixon et al. (1979).

Figure 8 shows the time history of instantaneous vorticity (ω) contour plots within one wave period cycle for Case S1. The red contour lines indicate the positive ω (counter-clockwise) and the blue contour lines indicate the negative ω (clockwise). It is clearly seen that the waves are diffracted by the cylinder and the vortices are separated after the waves travel over the cylinder. Flow separation is obviously observed at the bottom of the cylinder (see Figs. 8c and 8d), indicating the existence of viscous energy dissipation.

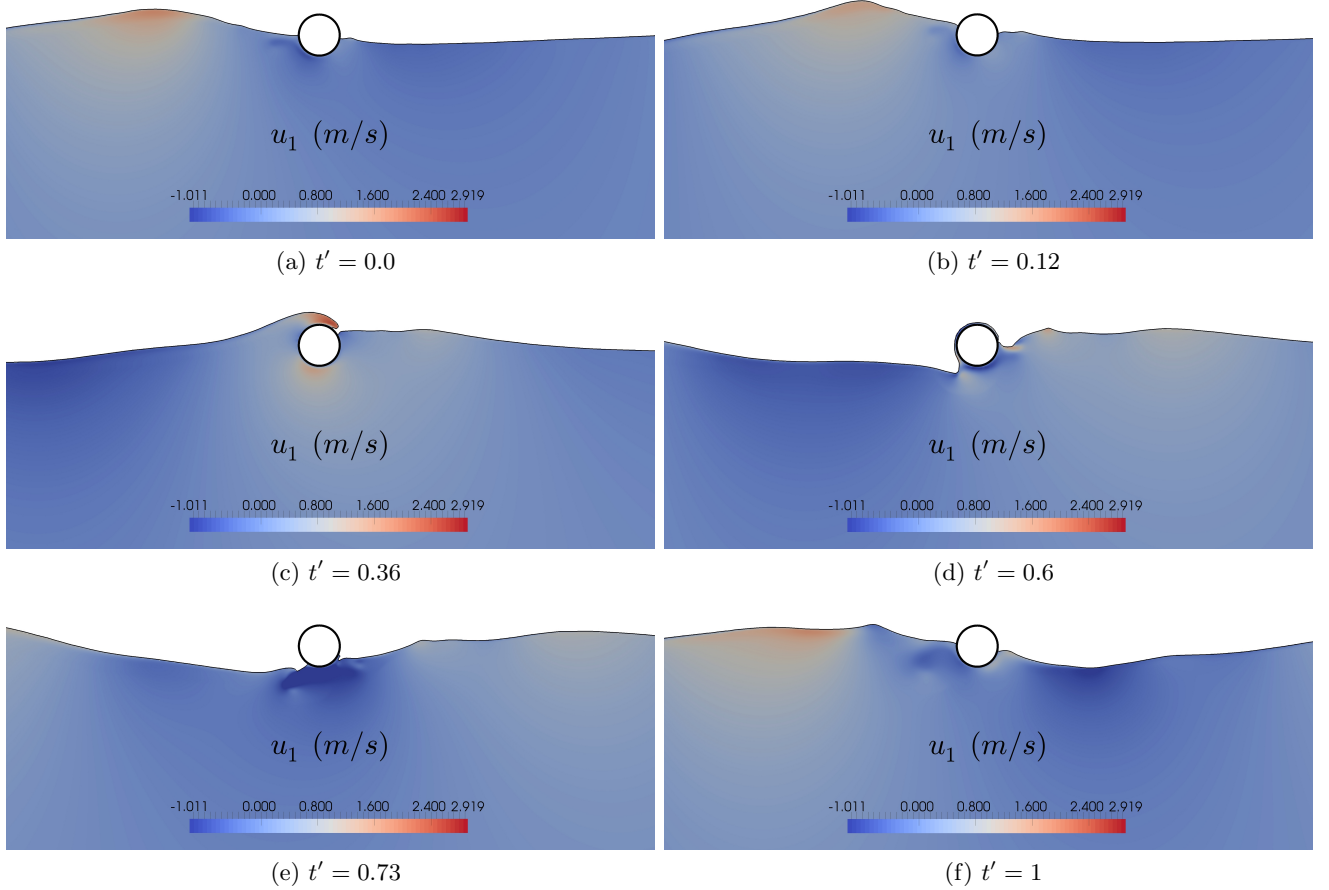


Figure 7: Time history of free surface elevation over a wave period for Case S1. The water domain is colored by 256 contours from -1.011 to 2.919 m/s

For $d' = 0$ and $a' = 0.2$ (Case S2), the cylinder is always partially-submerged during every wave period. Figure 9a shows F'_v versus t' over one wave period for Case S2. The feature of asymmetric force distribution over one wave period is also observed in this case (see also Dixon et al. (1979)). This is mainly due to the wave run-up on the cylinder. The wave over-topping action does not occur in this case. Therefore, there is a smooth decrease of F'_v beyond the positive peak of F'_v . It appears that the present results are generally in good agreement with the experiment measurements by Dixon et al. (1979). The maximum positive and negative values of F'_v are predicted reasonably well by the present simulation. For Case S3, the cylinder is then moved down to the position of $d' = -0.2$ and $a' = 0.2$ is kept. Both wave over-topping and run-up actions can occur in this case. F'_v versus t' over one wave period for Case S3 is shown in Figure 9b. Generally, the present model is able to capture the whole F'_v distribution well as compared to the experimental measurements. Small discrepancies are seen at the time near $t' = 0.73$, where values of F'_v have the largest negative value. For this case, the agreement between the present simulation and the experimental data appears to be better than that of Case S1. This is because the degree of wave over-topping action in Case S3 is less than that in Case S1, i.e. smaller value of a' with respect to d' in Case S3 than that

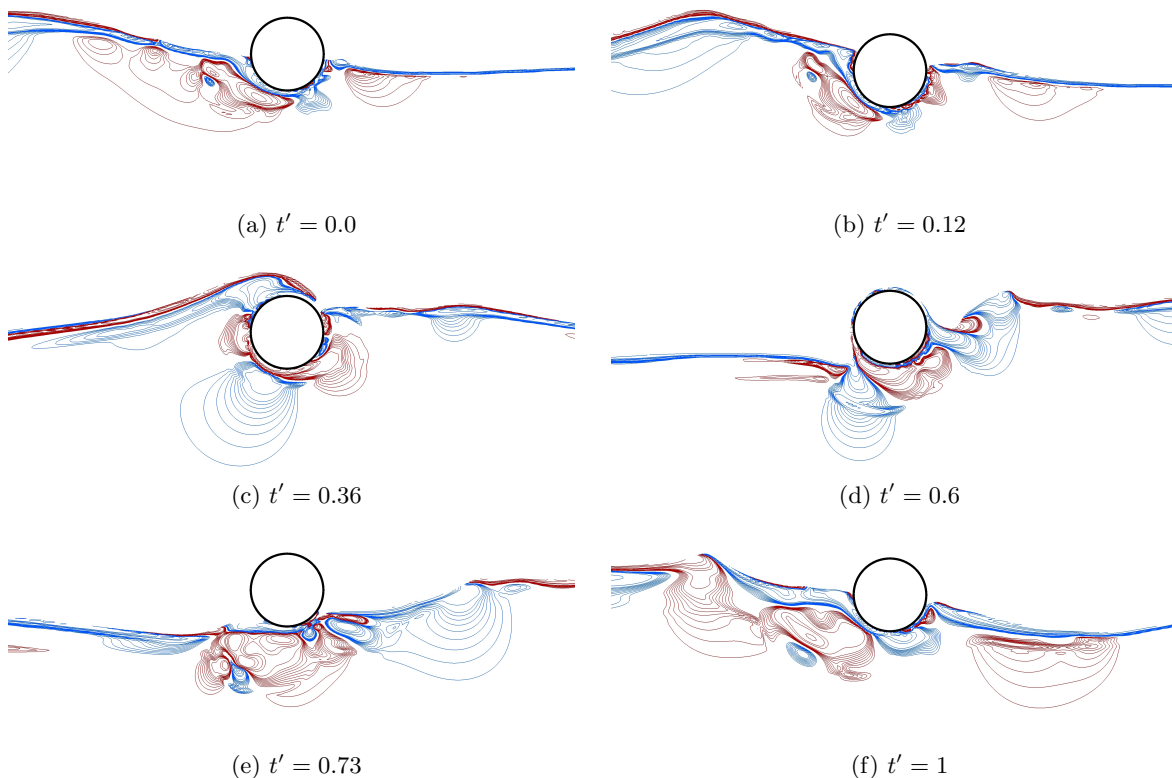


Figure 8: Time history of instantaneous vorticity (ω) over a wave period for Case S1. The red contour lines indicate the positive ω (counter-clockwise) and the blue contour lines indicate the negative ω (clockwise). 34 vorticity contours are plotted from -20 Hz to 20 Hz.

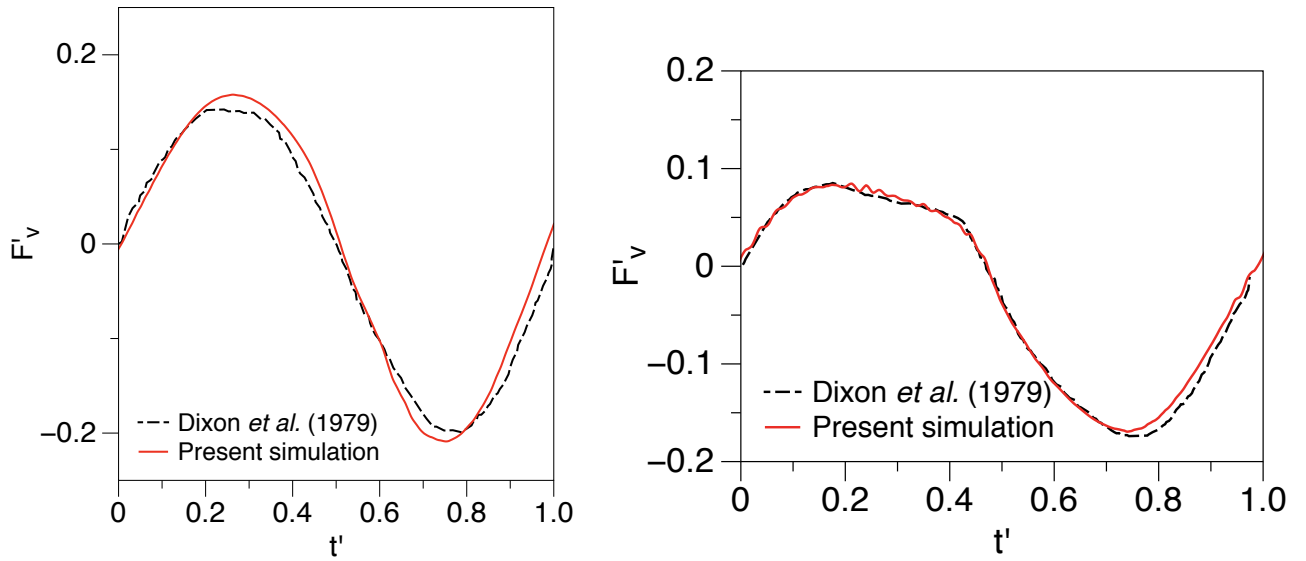
in Case S1.

Overall it appears that the present numerical model is able to predict the free surface waves past a partially-submerged cylinder reasonably well. These results are taken as a validation study for the subsequent investigation on the free surface waves past two semi-submerged cylinders in tandem, see Section 4.2.

4.2 Free Surface Waves past Two Semi-Submerged Horizontal Cylinders in Tandem

Similar numerical setup as for the cases of a single partially-submerged horizontal cylinder is employed to investigate the free surface waves past two semi-submerged horizontal cylinder in tandem, see Table 2 for the cases and Figure 3 for the definition sketch.

Figure 10 shows F'_v versus t' over one wave period for Case T1 ($a'=0.5$, $d'=0$, $S/D=1$), and the result of the single cylinder case S1 are also included for discussion. The free surface elevations around the two cylinders over one wave period $t' = (0, 0.12, 0.36, 0.6, 0.73, 1)$ are shown in Figure 11. In Figure 10, it is clearly seen that there is a phase difference between the time-history F'_v results over a wave period of the two cylinders due to their different horizontal locations. Owing to the existence of Cylinder 2 at the downstream location, the Cylinder 1 at the upstream location experiences a larger positive peak of F'_v as compared to



(a) F'_v versus t' over one wave period for Case S2

(b) F'_v versus t' over one wave period for Case S3

Figure 9: F'_v versus t' over one wave period for Case S2 and Case S3

the results of Case S1 for the single cylinder. This is physically sound because the spacing between Cylinder 1 and Cylinder 2 is small (i.e. $S/D = 1$); and the effect of flow blockage becomes significant. This makes wave run-up and over-topping actions on Cylinder 1 become more prominent. Therefore, generally Cylinder 1 experiences larger positive F'_v than that for

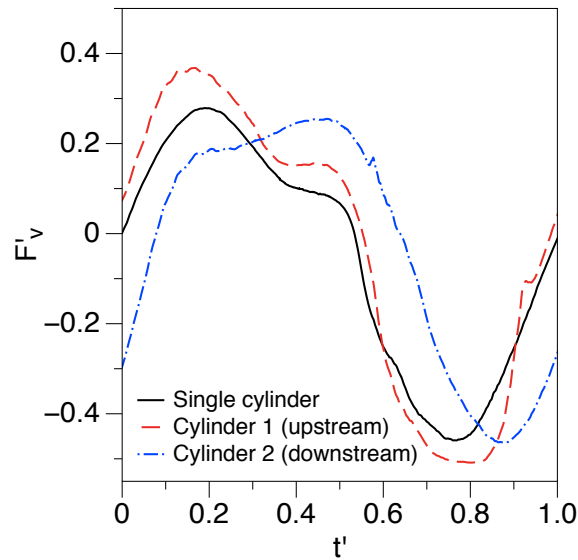


Figure 10: F'_v versus t' over one wave period for Case T1

the Case S1 (the single cylinder) for $t' < 0.6$. In Figure 11b, the water is trapped at the area between the two cylinders. This makes the F'_v distribution of Cylinder 2 different from that of Cylinder 1, see Figure 10. This trapped water between the two cylinders (see Figure 11c and 11d) leads to Cylinder 2 experiencing larger positive F'_v for a longer duration as compared to Cylinder 1. Due to the blocking effect caused by Cylinder 1, only wave run-up action is observed on Cylinder 2 throughout the wave period, see Figures 10 and 11.

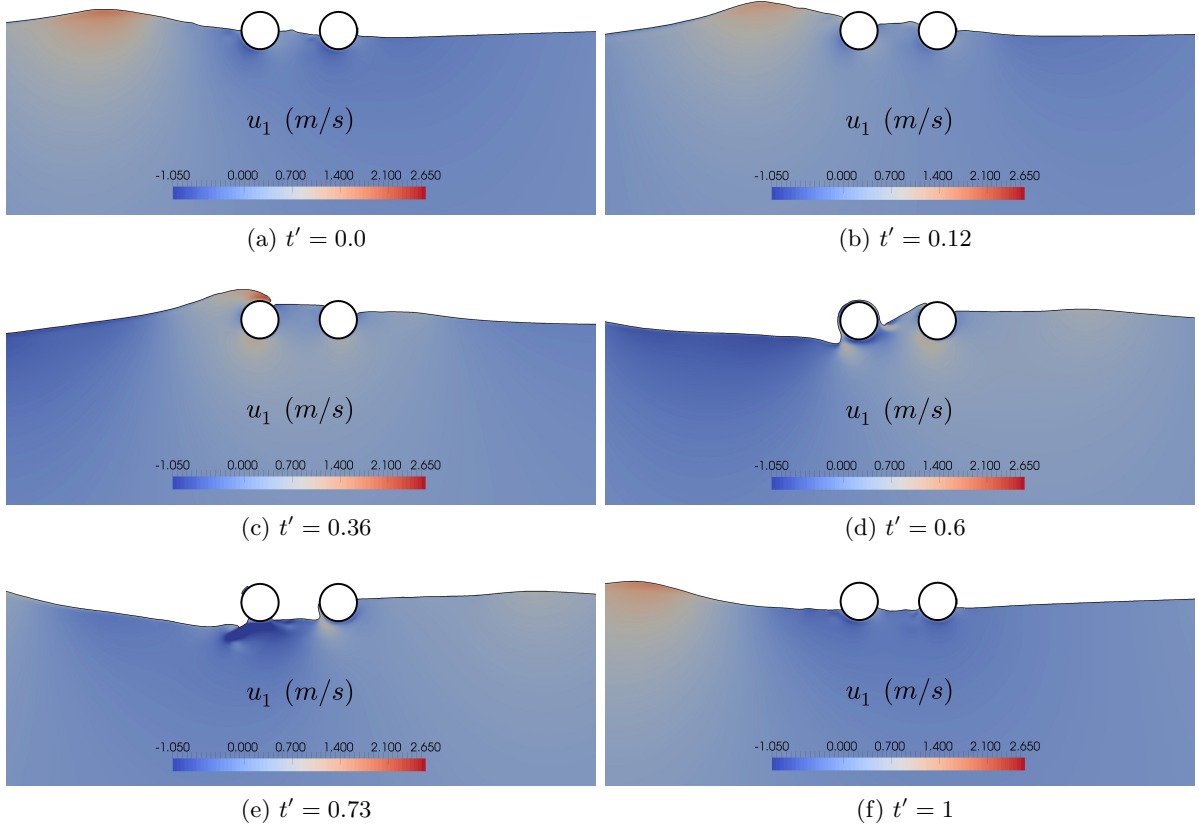


Figure 11: Time history of free surface elevation over a wave period for Case T1. The water domain is colored by 256 contours from -1.050 to 2.650 m/s

Figure 12 shows F'_v versus t' over one wave period for Case T2 ($a' = 0.5$, $d' = 0$, $S/D = 3$), including the result of the single cylinder case S1 for comparison. The free surface elevations around the two cylinders over one wave period $t' = (0, 0.12, 0.36, 0.6, 0.73, 1)$ for Case T2 are shown in Figure 13. By comparing Figure 10 and Figure 12, the wave run-up effect on Cylinder 1 caused by Cylinder 2 for $S/D = 3$ is less pronounced than that for $S/D = 1$. The maximum positive F'_v of Cylinder 1 is almost the same as that of Case S1 (the single Cylinder). This is physically sound because the spacing between two cylinders becomes larger; and Cylinder 2 creates less blockage of flow. Subsequently, less significant wave run-up effect on Cylinder 1 during the first half wave period is observed. For $0.3 < t' < 0.7$, the water is being trapped between the two cylinders (see Figures 13c-13e), mainly because S/D is still small. Again, this trapped water causes Cylinder 2 experiencing a longer duration of positive F'_v than Cylinder 1. By comparing the F'_v results between Cylinder 2 for T1 (Figure 10) and Cylinder 2 for T2

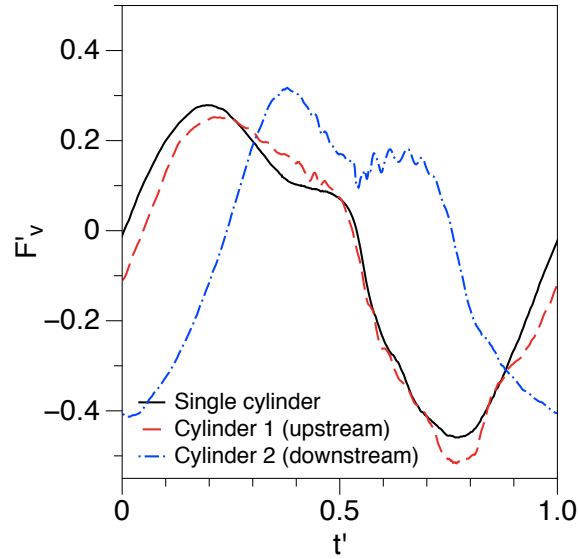
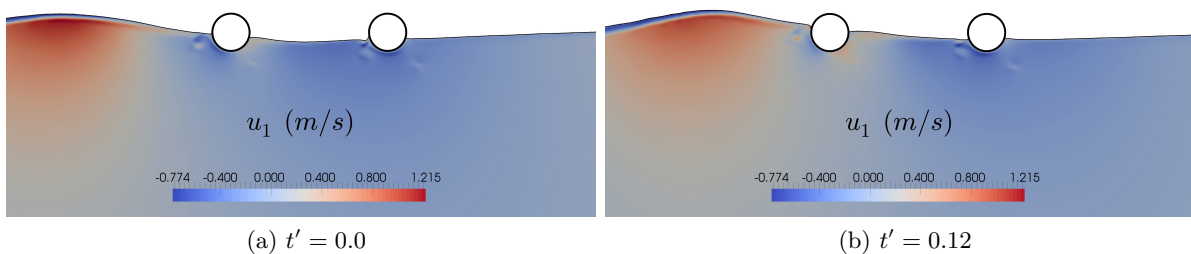


Figure 12: F'_v versus t' over one wave period for Case T2

(Figure 12), it is found that the water between two cylinders is trapped for a longer duration for T2 than that for T1. At $t' = 0.73$ in Figure 12, Cylinder 1 experiences a larger magnitude of negative F'_v as compared to that of the single cylinder Case S1. This is because the free surface waves are reflected upstream after hitting Cylinder 2; and subsequently the reflected waves further reduce the free surface elevation around Cylinder 1. Same as Case T1, only wave run-up action is observed on Cylinder 2 throughout the wave period.

Figure 14 shows the time history of instantaneous vorticity (ω) contour plots over one wave cycle for Case T2. The red contour lines indicate the positive ω (counter-clockwise) and the blue contour lines indicate the negative ω (clockwise). The waves are diffracted due to Cylinder 1. Vortices are generated around the cylinders and this contributes to significant viscous damping. Cylinder 2 experiences the diffracted waves from Cylinder 1. Due to the low KC number, it appears that the wakes generated by Cylinder 1 do not travel to the location of Cylinder 2. A flow separation feature is clearly observed at the bottom side of Cylinder 2.

F'_v versus t' over one wave period for Case T3 ($a' = 0.5$, $d' = 0$, $S/D = 7$) is shown in Figure 15 together with the result of the single cylinder case S1. The free surface elevations around the two cylinders over one wave period $t' = (0, 0.12, 0.36, 0.6, 0.73, 1)$ for Case T3 are shown



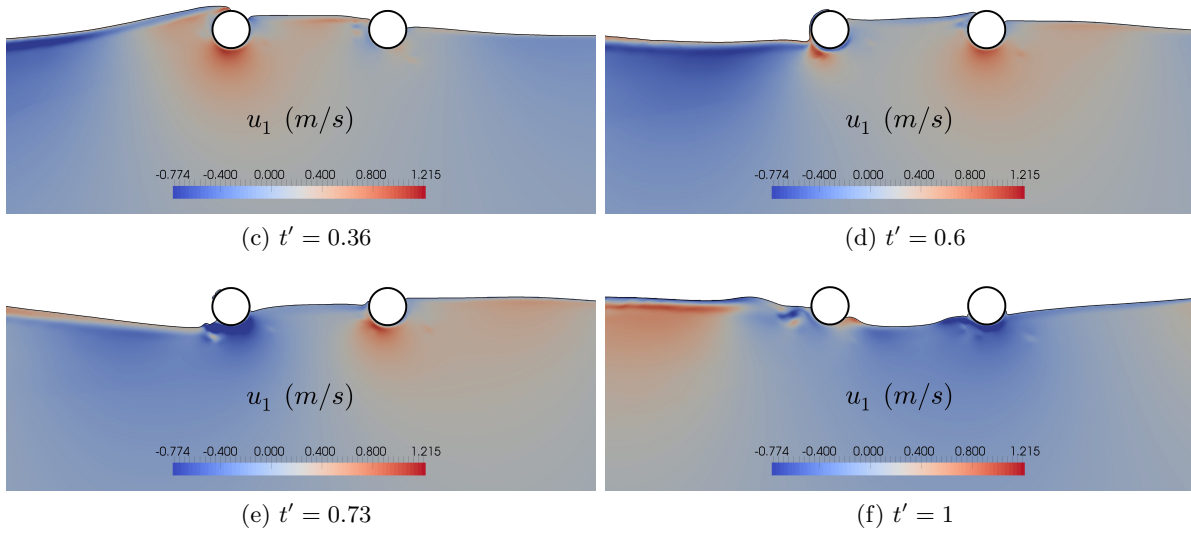


Figure 13: Time history of free surface elevation over a wave period for Case T2. The water domain is colored by 256 contours from -1.050 to 2.650 m/s

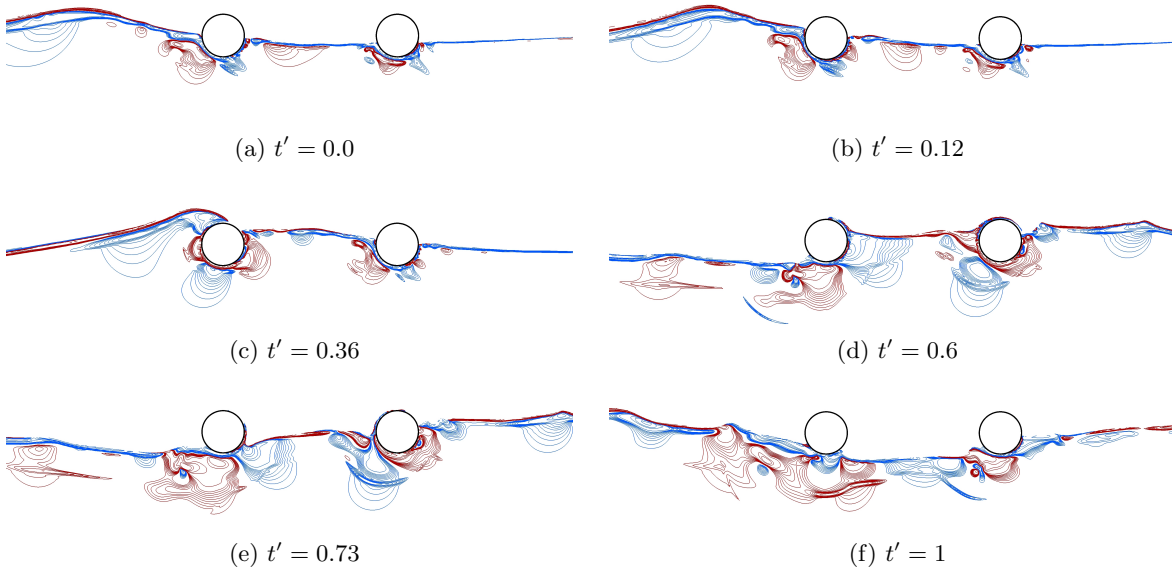


Figure 14: Time history of instantaneous vorticity (ω) over a wave period for Case T2. The red contour lines indicate the positive ω (counter-clockwise) and the blue contour lines indicate the negative ω (clockwise). 34 vorticity contours are plotted from -20 Hz to 20 Hz.

in Figure 16. In Figure 15, It is observed that the time-history F'_v results over a wave period of Cylinder 1 and Cylinder 2 are out of phase. This is physically correct because the spacing between two cylinders is close to half of the investigated wave length (i.e. $L'=15.62$). For $t' < 0.5$, it is observed that, due to a large spacing between two cylinders, the influence of Cylinder 2 on the wave run-up effect of Cylinder 1 is much less as compared to those observed

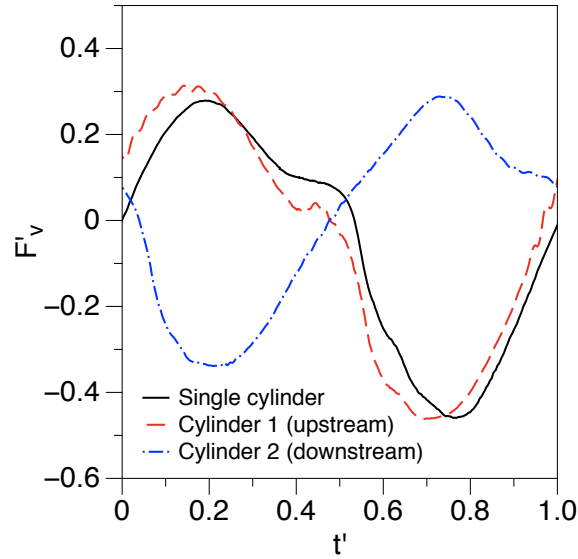
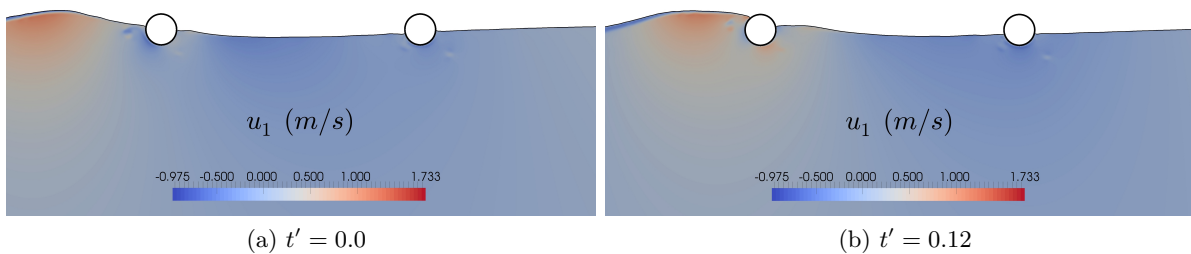


Figure 15: F'_v versus t' over one wave period for Case T3

in Case T1 (Figure 10) and Case T2 (Figure 12). By observing the free surface elevation results in Figure 16, no excessive water is trapped between the two cylinders. Same as previous cases, only wave run-up action is observed on Cylinder 2 throughout the wave period.

Figure 17 shows F'_v versus t' over one wave period for Case T4 ($a' = 0.5$, $d' = 0$, $S/D = 15$), and the result of the single cylinder case S1 is also included for discussion. It should be noted that the spacing between the two cylinders ($S/D = 15$) is almost equal to one wave length of the incident waves ($L' = 15.62$). The present simulation results shows that the time-history F'_v results over one wave period of Cylinder 1 and Cylinder 2 are in phase with each other; and this feature is physically sound. Due to the large spacing between the two cylinders, the time history F'_v results of Cylinder 1 almost coincides with the results of the single cylinder Case S1. Figure 18 shows the free surface elevations around the two cylinders over one wave period $t' = (0, 0.12, 0.36, 0.6, 0.73, 1)$ for Case T4. It is obviously seen that the variation of the free surface elevation around Cylinder 2 is less significant than that around Cylinder 1. Figure 17 also shows that the magnitude of the negative F'_v of Cylinder 2 is less than that of Cylinder 1. This is mainly because the wave activity has partially been damped out due the viscous energy dissipation due to the flow separation and the existence of wave diffraction at



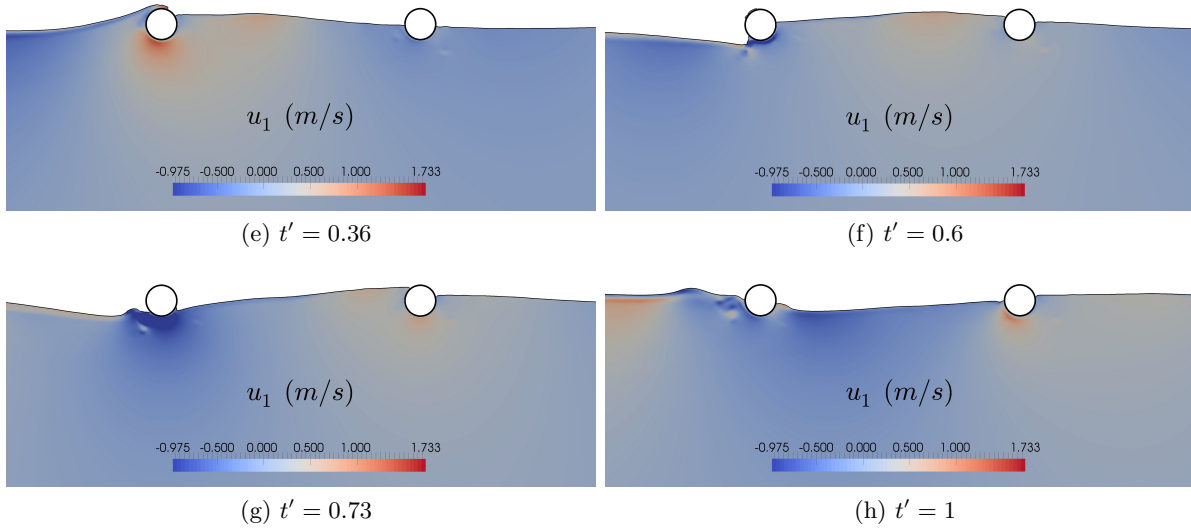


Figure 16: Time history of free surface elevation over a wave period for Case T3. The water domain is colored by 256 contours from -0.975 to 1.733 m/s

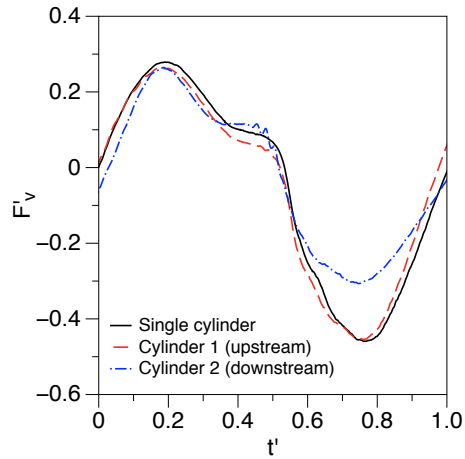


Figure 17: F'_v versus t' over one wave period for Case T4

Cylinder 1.

Overall it appears that the present numerical model is suitable for predicting the hydrodynamic quantities and the corresponding free surface elevations based on the present investigation of free surface waves past partially submerged cylinders.

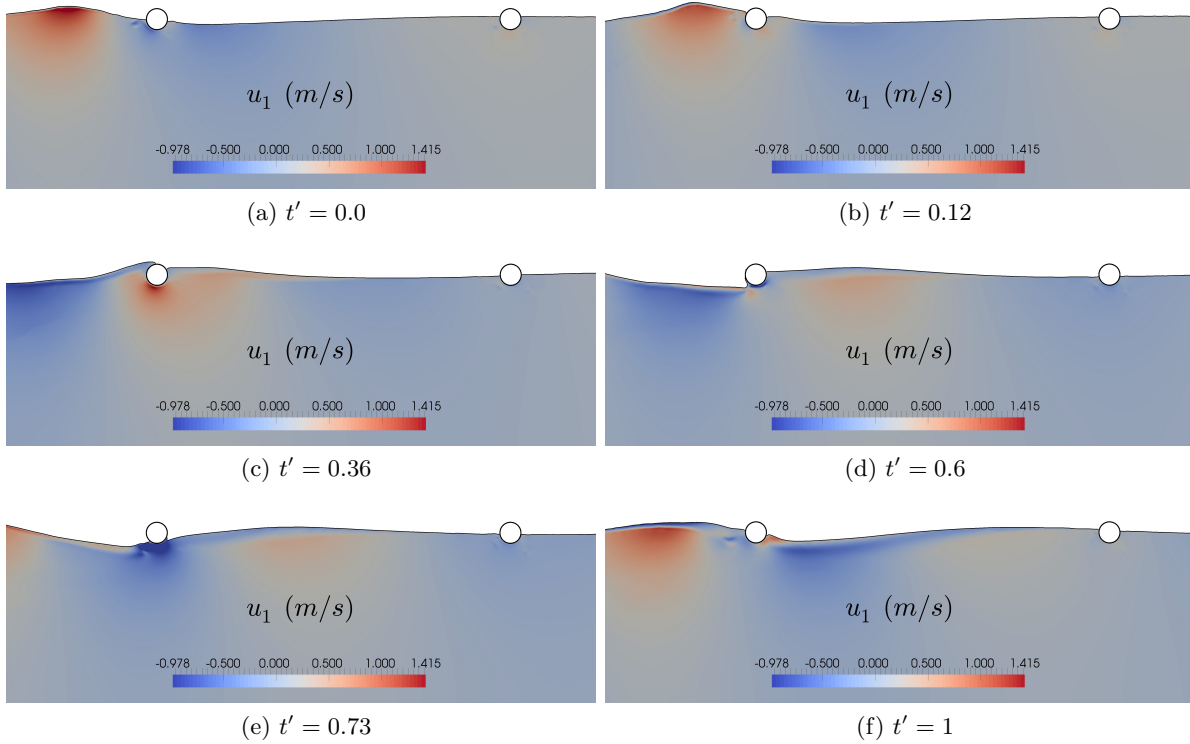


Figure 18: Time history of free surface elevation over a wave period for Case T4. The water domain is colored by 256 contours from -0.978 to 1.415 m/s

5 Conclusions

Free surface regular waves past partially-submerged horizontal circular cylinders under deep water conditions have been studied numerically by solving URANS equations together with the $k-\omega$ turbulence model and level set method for the free surface modeling. The main results are summarised as follows:

(a) Free Surface Waves past a Partially-Submerged Horizontal Cylinder

The present predicted vertical wave forces on the cylinder (F'_v) have been compared directly with the published experimental data by Dixon *et al.* (1979). Overall, the present model is able to predict the time-history F'_v results over one wave period well for the cases with cylinders at different submerged depth subject to various incident wave properties. The present model predicts both maximum positive and negative F'_v and asymmetric F'_v distribution over one wave period well as compared with the experimental data. The present model is able to predict the wave run-up and over-topping actions around the cylinder with reasonable explanation from the time history F'_v results. This work is used as a validation study for the further investigation on the free surface waves past two semi-submerged horizontal cylinder in tandem.

(b) Free Surface Waves past Two Semi-Submerged Horizontal Cylinders in Tandem

Wave forces and free surface elevations around two semi-submerged horizontal cylinders in tandem have been predicted numerically by varying the spacing between the cylinders. For the cases with small spacing (i.e. $S/D = 1$ and 3) between the two cylinders, more prominent wave run-up and over-topping actions and larger positive F'_v on Cylinder 1 (upstream) are observed as compared with that of the single cylinder case. This is mainly attributed to the blocking effects caused by Cylinder 2 (downstream). Moreover, the water trapped between the two cylinders causes Cylinder 2 experiencing larger positive F'_v for a longer duration as compared to Cylinder 1.

When S/D is about half of the wave length, the time-history F'_v results over a wave period of Cylinder 1 and Cylinder 2 are out of phase. When S/D is about one wave length, the time-history F'_v of Cylinder 1 and Cylinder 2 are in phase with each other. For larger S/D , no excessive water is trapped between the two cylinders; hence, the time history F'_v results of Cylinder 1 are similar to the results of the single cylinder. The variation of the free surface elevation around Cylinder 2 is less significant than that around Cylinder 1 because the wave activity has partially been damped out by Cylinder 1.

Overall it appears that the present numerical model is suitable for predicting the hydrodynamic quantities and the corresponding free surface elevations based on the present investigation of free surface waves past partially submerged cylinders. However, more experimental data are required in order to perform a further detailed validation study of the model. Moreover, the present work can be used as a validation study for the future work on wave-induced motions of bluff bodies.

Acknowledgements

This research has been carried out under “OWC Wave Energy Converters for Combined Clean Energy and Coastal Protection” (Project No: 217622/E20) and the authors are grateful to the grants provided by the Research Council of Norway. This study was supported in part with computational resources at the Norwegian University of Science and Technology (NTNU) provided by the Norwegian Metacenter for Computational Science (NOTUR), under Project No. NN2620K.

References

- Alagan Chella, M., Bihs, H. and Myrhaug, D. (2015*a*). Characteristics and profile asymmetry properties of waves breaking over an impermeable submerged reef. *Coastal Engineering*, **100**, 26–36.
- Alagan Chella, M., Bihs, H., Myrhaug, D. and Muskulus, M. (2015*b*). Hydrodynamic characteristics and geometric properties of plunging and spilling breakers over impermeable slopes. *Ocean Modelling, Virtual Special Issue: Ocean Surface Waves*, 1–20.
- Berthelsen, P.A. and Faltinsen, O.M. (2008). A local directional ghost cell approach for

- incompressible viscous flow problems with irregular boundaries. *Journal of Computational Physics*, **227**, 4354–4397.
- Chorin, A. (1968). Numerical solution of the Navier Stokes equations. *Mathematics of Computation*, **22**, 745–762.
- Dixon, A.G., Greated, C.A. and Salter, S.H. (1979). Wave forces on partially submerged cylinders. *Journal of the Waterway Port Coastal and Ocean Division*, **105**(4), 421–438.
- Easson, W.J., Greated, C.A. and Duranni, T.S. (1985). Force spectra from partially submerged circular cylinders in random seas. *Journal of the Waterway Port Coastal and Ocean Division*, **111**(5), 856–879.
- Engsig-Karup, A.P. (2006). *Unstructured Nodal DG-FEM Solution of High-order Boussinesq-type Equations*. Ph.D. thesis, Technical University of Denmark, Lyngby.
- Hu, Z.Z., Causon, D.M., Mingham, C.G. and Qian, L. (1985). Numerical simulation of floating bodies in extreme free surface waves. *Natural Hazards and Earth System Sciences*, **11**, 519–527.
- Jacobsen, N.G., Fuhrman, D.R. and Fredsøe, J. (2012). A wave generation toolbox for the open-source CFD library : OpenFOAM. *International Journal for Numerical Methods in Fluids*, **70**, 1073–1088.
- Jiang, G.S. and Shu, C.W. (1996). Efficient implementation of weighted ENO schemes. *Journal of Computational Physics*, **126**, 202–228.
- Kamath, A., Alagan Chella, M., Bihs, H. and Arntsen, Ø.A. (2015a). Cfd investigations of wave interaction with a pair of large tandem cylinders. *Ocean Engineering*, **108**, 738–748.
- Kamath, A., Bihs, H. and Arntsen, Ø.A. (2015b). Numerical investigations of the hydrodynamics of an oscillating water column device. *Ocean Engineering*, **102**, 40–50.
- Larsen, J. and Dancy, H. (1983). Open boundaries in short wave simulations - a new approach. *Coastal Engineering*, **7**, 285–297.
- Mayer, S., Garapon, A. and Sørensen, L.S. (1998). A fractional step method for unsteady free surface flow with applications to non linear wave dynamics. *International Journal for Numerical Methods in Fluids*, **28**, 293–315.
- Osher, S. and Sethian, J.A. (1988). Fronts Propagating with Curvature-Dependent Speed: Algorithms Based on Hamilton-Jacobi Formulations. *Journal of Computational Physics*, **79**, 12–49.
- Prasad, S. (2011). Three-dimensional numerical modeling of local scouring in open channel flow. PhD thesis.
- Shu, C.W. and Osher, S. (1988). Efficient implementation of essentially non-oscillatory shock capturing schemes. *Journal of Computational Physics*, **77**, 439–471.

- van der Vorst H. (1992). BiCGStab: A fast and smoothly converging variant of Bi-CG for the solution of nonsymmetric linear systems. *SIAM Journal on scientific and Statistical Computing*, **13**, 631–644.
- Westphalen, J., Greaves, D.M., Williams, C.K. and Taylor, P.H. (2009). Extreme wave loading on offshore wave energy devices using CFD. In: *Proceedings of the 8th European Wave and Tidal Energy Conference*.
- Wilcox, D.C. (1994). *Turbulence Modeling for CFD*. DCW Industries Inc., La Canada, California.